

Superior Performances of Q-Switched and Mode-Locked Erbium-doped Fiber Laser using Black Titanium Dioxide Thin-film Saturable Absorbers

A. R. Johari^{a,b}, H. Bakhtiar^{a,b}, S. Daud^{a,b}, G. Krishnan^{a,b*}

^aLaser Center, Ibnu Sina Institute for Scientific and Industrial Research, Universiti Teknologi Malaysia, 81310 UTM Johor Bahru, Johor, Malaysia; ^bDepartment of Physics, Faculty of Science, Universiti Teknologi Malaysia, 310 UTM Johor Bahru, Johor, Malaysia

Abstract This work reports on the improved Q-switched and mode-locked performances of black titanium dioxide (BTiO_{2-x}) nanoparticles embedded in thin-film composite material as a saturable absorber compared to TiO₂ in an erbium-doped fiber laser. The thin-film saturable absorbers were prepared by mixing the nanoparticles with polyvinyl alcohol (PVA) as a host. BTiO_{2-x} has a better nonlinear absorption coefficient, β of -12.46×10^{-7} m/W compared to -7.15×10^{-7} m/W for TiO₂ determined using z-scan measurement. The laser performance was evaluated in the 85.21 mW – 126.48 mW pump power range. Upon inserting TiO₂ and BTiO_{2-x} SA in a laser cavity, the peaks of the output spectrum shifted from 1566.62 nm to 1563.24 nm and 1565.75 nm, respectively. Regarding Q-switched performances, BTiO_{2-x} SA generates a shorter pulse width of 16.00 μ s than TiO₂ SA. The slope efficiency of the TiO₂ SA was 11.72 %, which is higher than the slope efficiency of the BTiO_{2-x} SA. The maximum average and peak power generated by the BTiO_{2-x} SA were 55.67 % and 54.83 % higher than the TiO₂ SA. As for mode-locked outputs, BTiO_{2-x} SA can generate pulsed laser at a low threshold power of 62.29 mW compared to TiO₂ SA. Furthermore, BTiO_{2-x} SA produced a shorter pulse width of 5.04 ps, whereas TiO₂ is 9.20 ps. This study demonstrates that BTiO_{2-x} SA has the potential to produce ultrashort pulse width using the mode-locked technique.

Keywords: Saturable absorber, fiber laser, black titanium dioxide, q-switch, mode-locked.

Introduction

Fiber laser technology has been used widely in major industries such as medical [1], [2], telecommunication [3], [4], and machinery [5] industries. Industries use a pulsed laser system due to its high peak power and short pulse width. Q-switched and mode-locking techniques are required to generate pulsed lasers. Q switching creates intense short light pulses from a laser by adjusting the intracavity losses and, subsequently, the laser resonator's Q factor. These techniques need a saturable absorber (SA) as one of the main components in the laser system. A passive SA is favorable to an active SA because of its simple implementation in laser systems. An active SA needs an external trigger to produce a pulsed laser, while a passive SA can be directly applied to the laser cavity without any additional devices. Much research is dedicated to producing SA materials to generate higher pulsed energy lasers [3].

Various SA materials have been discovered and applied in fiber laser systems. Recent research has discovered new MXene and Max phase family compounds SA materials. They can generate a maximum output power of 8.17 mW in an erbium-doped fiber laser [6]. One of the common materials used in pulsed laser systems is Semiconductor saturable-absorber mirrors (SESAM). SESAM can produce 8.37 mW of maximum average output power using the input power of 46.75 mW with an efficiency of 29.4% [7].

***For correspondence:**
k.ganesan@utm.my

Received: 24 Sept. 2023
Accepted: 19 Dec. 2023

©Copyright Johari. This article is distributed under the terms of the [Creative Commons Attribution License](#), which permits unrestricted use and redistribution provided that the original author and source are credited.

However, the production of SESAM is complicated and needs specialised equipment, causing its price to be high [8]. A few years later, researchers developed graphene as an SA material because of its nearly zero bands, so that it can be operated in almost all regions [9]. Luo *et al.* discovered that laser pulse energy could generate up to 16.7 nJ using a graphene SA [10]. Unfortunately, graphene SA has a low modulation depth, whereas a high modulation depth is an essential characteristic of an SA material. Next, black phosphorous (BP) SA was discovered, and the maximum laser pulse energy produced with a BP SA was 18.6 nJ [11]. Unfortunately, the major drawback of BP SA was its hydrophilic nature [12], [13]. As a result, it required an airtight box to prevent it from exposure to moisture.

Titanium dioxide or titania (TiO_2) has been used in applications such as the production of paint and sunscreen. Researchers have been researching TiO_2 to discover its applications in optics [14]. Recently, researchers found that TiO_2 has the potential to be used as an SA material due to a fast recovery time of around ~ 1.5 ps [15], [16]. Due to its abundance, TiO_2 is cost-effective for SA applications compared to recently discovered MXene and Max phases SAs. Yusoff *et al.* used TiO_2 recovered from natural Malaysian ilmenite waste as the SA and produced a laser output pulse with an energy of 47.5 nJ using a pump power of 57.0 mW [17]. This result shows an increase in pulse energy by about 60 % compared to BP SA. Ahmad *et al.* demonstrated that a pulsed laser output with a repetition rate of 81.04 kHz to 90.58 kHz was generated with TiO_2 SA in an EDF laser [18].

BTiO_{2-x} , also known as hydrogenated TiO_2 , is a form of TiO_2 with some degree of defects on the particle's surface. It is synthesized through the hydrogenation process of TiO_2 [19] and chemical reduction methods [20]. BTiO_{2-x} has higher absorption in the UV-visible wavelength region than TiO_2 [21]. In terms of the nonlinear optical properties of BTiO_{2-x} , Zhang *et al.* reported that BTiO_{2-x} has a three times higher order of nonlinear optical absorption coefficients than TiO_2 [21]. Due to its high nonlinear absorption coefficient, BTiO_{2-x} is a perfect candidate for the SA application. Nevertheless, the potential of BTiO_{2-x} as SA has not been explored.

This report applies TiO_2 and BTiO_{2-x} SA as passive SA sandwiched between fiber ferrules in a laser cavity to generate Q-switched and mode-locked in the Erbium-doped fiber laser (EDFL). We used Polyvinyl alcohol (PVA) as the host for TiO_2 and BTiO_{2-x} nanoparticles to produce thin-film SAs using the airbrush method. As a result, superior laser performance was achieved using BTiO_{2-x} SA, producing higher output pulse energy than TiO_2 SA.

Thin-film Saturable Absorber Preparation

Before the thin-film SA production, the TiO_2 and BTiO_{2-x} nanoparticles powders were characterised using the X-Ray diffraction (XRD) technique to verify their structural properties. The airbrush spraying method was applied to control the thickness of the thin-film SA produced, where the SA behaviors change with the thin film's thickness [11]. The first step in this work was thin-film SA preparation. Initially, we used TiO_2 nanoparticles as the subject for the thin film sample. Firstly, at room temperature, 0.03 g of TiO_2 powder and 15 ml of distilled water were mixed for an hour using a magnetic hot plate stirrer. Then, the mixture was put into an ultrasonic bath for 30 minutes to ensure the TiO_2 was blended well with the distilled water. In the meantime, PVA solution was prepared by mixing 1 g of PVA powder with 120 ml of distilled water as a solvent. TiO_2 -distilled water solution was then mixed with PVA solution with a ratio of 15 ml:7.5 ml. After that, the mixed TiO_2 -PVA solution was stirred for an hour using a magnetic hot plate stirrer and then put into an ultrasonic bath for 30 minutes.

Before starting the airbrush process, acrylic plate sides were polished using sandpaper. Then, the acrylic plate was put into an ultrasonic bath for 15 minutes. After that, the acrylic was wiped using optical lens tissue. Next, the TiO_2 -PVA solution was placed in an airbrush container for spray deposition. The airbrush setup was connected to a tube from the argon gas tank that provided 50 kPa of argon gas pressure, by which the solution drip rate was maintained, and the TiO_2 -PVA solution was automatically pulled from the solution chamber into the airbrush. A fixed distance of 10 cm was maintained between the spraying nozzle and the acrylic plate. During the airbrushing process, a hot plate was positioned underneath the acrylic plate to dry the droplets that landed on the plate. The spray coating process was repeated with a constant pattern to form 50 coating layers. Once the spray coating was completed, the coated acrylic was left to cool naturally at room temperature before peeling the thin film from the acrylic plate's surface. These thin-film SA preparation steps were repeated to prepare a BTiO_{2-x} thin film. Figure 1 below summarises the steps to produce the thin-film SAs. The thin-film SAs were characterised using UV-Vis spectroscopy and a scanning electron microscope (SEM) for their optical and morphological properties. The nonlinear absorption coefficient β values for thin-film SAs were determined using a single beam z-scan technique based on a 532 nm CW laser.

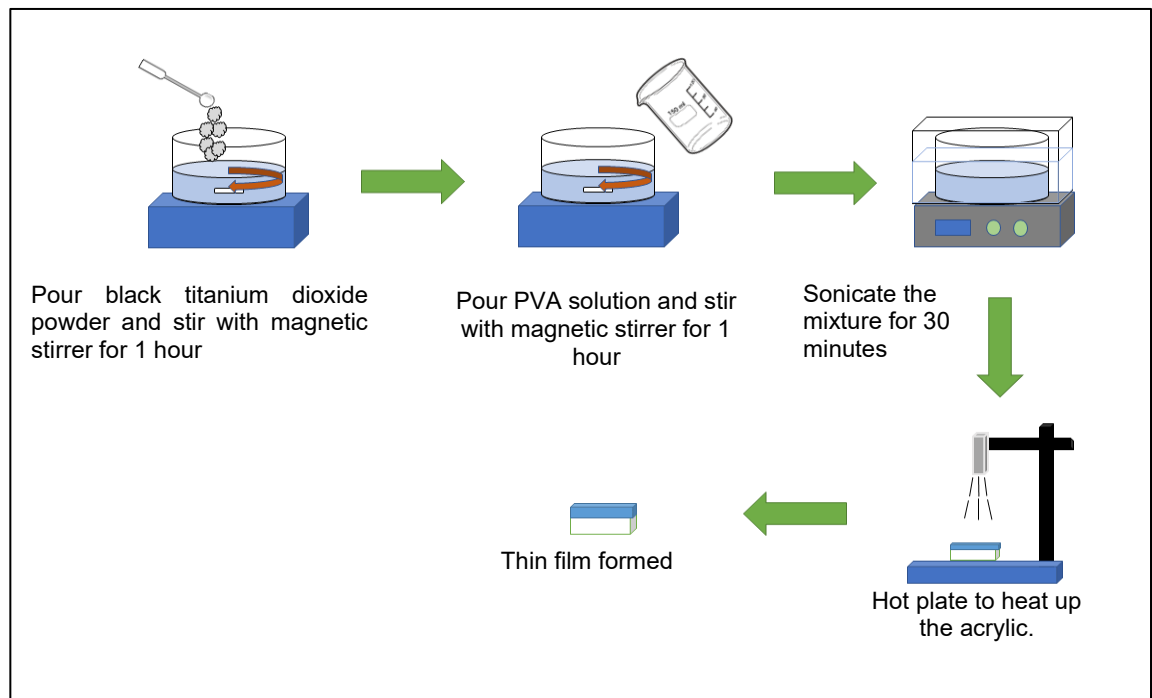


Figure 1. Preparation of TiO_2 and BTiO_{2-x} thin films

Experimental Setup

The pumping source for the laser cavity was a 976 nm laser diode. The pumping laser beam was coupled into the laser cavity using a 980/1550 nm wavelength division multiplexer (WDM). As shown in Figure 2, an erbium-doped fiber with a length of 2.4 m was used as the gain medium with a total cavity length of 6 m in the laser cavity. The EDF's numerical aperture (NA) was 0.2, and the core diameter was 5.8 μm . An isolator was added to the ring cavity to ensure the laser beam propagated in a single direction. The thin-film SA, which has a dimension of 1 mm x 1 mm, was sandwiched between two fiber ferrules with the help of an FC-to-FC adapter added to the ring cavity. An index-matching gel was added between the fiber ferrules and the SA to prevent parasitic reflections. Finally, a 90:10 coupling ratio output coupler was employed to transmit 10% of the signal out of the cavity for measurement. The Q-switched laser output was generated. A 100m single-mode fiber (SMF) was added to the cavity to generate mode-locked laser output, as shown in Figure 2. Therefore, the total cavity length of the mode-locked setup was 106 m.

A digital power meter, an optical spectrum analyser, a digital oscilloscope, a radio frequency spectrum analyser, and an autocorrelator were used to characterise the pulsed laser output. The output power of the pulsed laser was measured using the digital power meter (Thorlabs PM100D). The optical spectrum analyser (YOKOGAWA AQ6370D) with a resolution of 0.02 nm was used to characterise the laser optical spectrum. To capture the temporal features of the pulsed laser output, the 350 MHz digital oscilloscope (GWINSTEK, GDS-3352) and the 7.8 GHz radio frequency spectrum analyser (ANRITSU, MS2683A) were used, where the equipment was connected to the laser output fiber through an InGaAs photodetector.

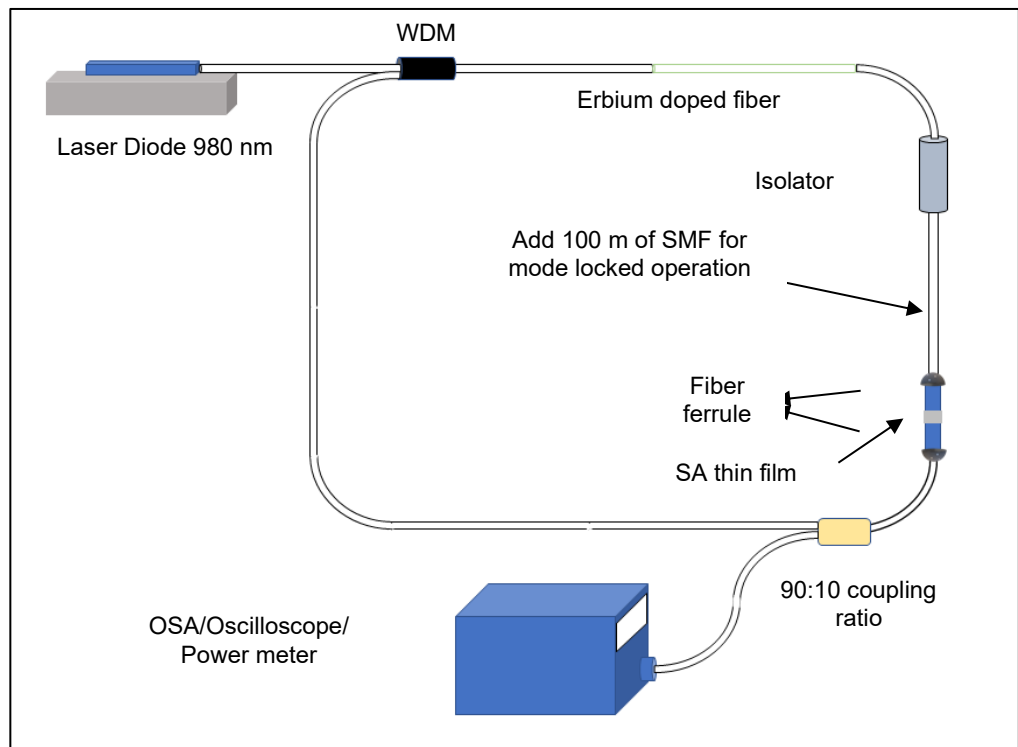


Figure 2. Experimental setup of EDF laser

Result and Discussion

Characterisation

The structural analysis of the BTiO_{2-x} and TiO_2 powders was carried out using the X-Ray diffraction (XRD) technique. XRD was helpful in ascertaining the samples' crystallographic structures and verifying the nature of the samples. Figure 3 shows the XRD patterns of BTiO_{2-x} and TiO_2 powders. For the TiO_2 sample, clear XRD peaks were acquired, which indicates the crystalline nature of the sample. The XRD pattern of TiO_2 sample fairly matches with the crystalline features of anatase (PDF card # 21-1272) [22]. The prominent diffraction peak observed at $2\theta = 25.29^\circ$ can be attributed to the (hkl) crystal planes of the sample, with the most probable Miller indices corresponding to (1 0 1) as supported by Chougala *et al.* [23]. On the other hand, the XRD pattern of BTiO_{2-x} sample shows clear XRD peaks that indicate the crystallinity of BTiO_{2-x} sample is significantly lower than the TiO_2 sample. This drop in the crystallinity happens during the production of BTiO_{2-x} powder through the reduction of TiO_2 with NaBH_4 [24].

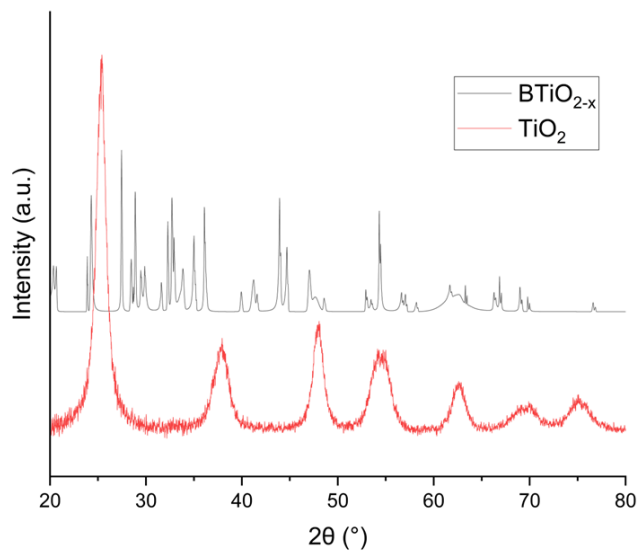


Figure 3. XRD patterns of BTiO_{2-x} and TiO₂ powders

UV-Vis spectroscopy was used to determine the linear absorption coefficient. This information was also required to calculate the nonlinear absorption coefficient. The absorption values at 1566 nm for the BTiO_{2-x} and TiO₂ SA are 4.328 a.u. and 4.745 a.u., respectively, as shown in Figure 4. This result shows that the BTiO_{2-x} SA has a superior linear absorption coefficient compared to TiO₂ SA. Figure 5 shows a scanning electron microscope (SEM) image of the TiO₂ thin-film SA cross-section. From the figure, the thin film formed using the airbrush technique has a mean thickness of 63.833 μm.

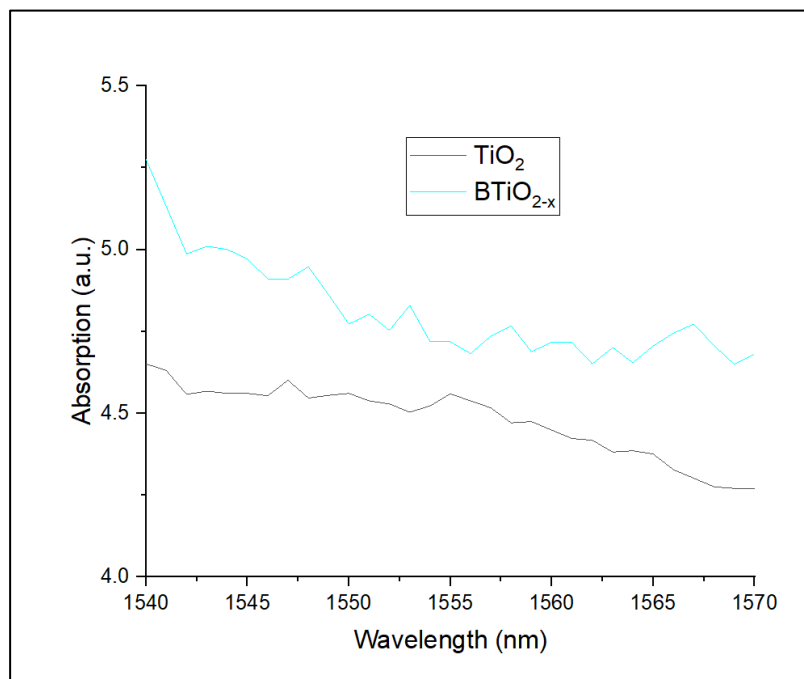


Figure 4. UV-Vis-NIR spectroscopy of TiO₂ and BTiO_{2-x}

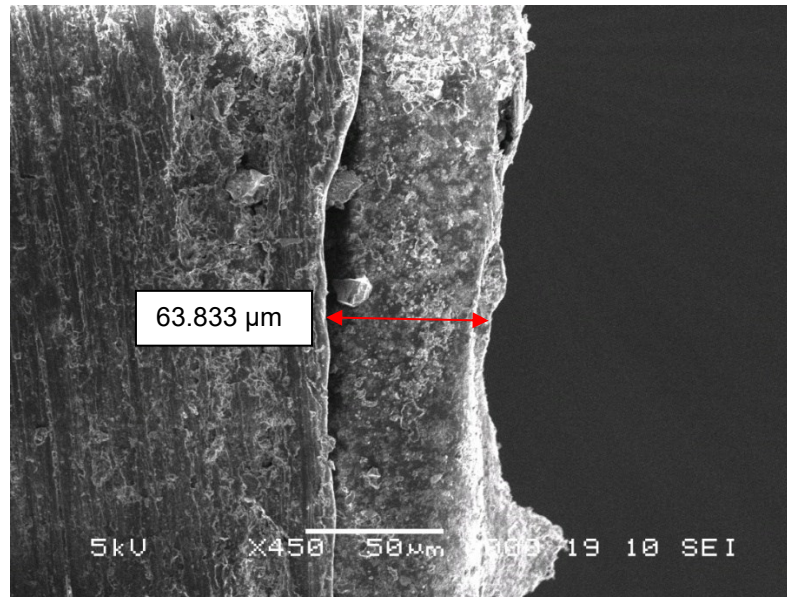


Figure 5. SEM image of thin film on the acrylic plate

Z-scan measurement was used to measure the nonlinear absorption coefficient of the thin-film SAs. The procedures of z-scan measurement were done according to Munzir *et al.* [25]. Figure 6 (a) and (b) clearly show the open aperture signals from BTiO_{2-x} and TiO₂, respectively. The open aperture signals show that both SAs have the saturable absorber behavior. From the analysis of the open aperture Z-scan measurement, BTiO_{2-x} SA has a higher nonlinear absorption coefficient, β , -12.46×10^{-7} m/W, which is higher than TiO₂ SA, -7.15×10^{-7} m/W, by 78%. The high nonlinear absorption coefficient of BTiO_{2-x} leads to enhanced nonlinear effects and broader possibilities for pulsed laser manipulation and control.

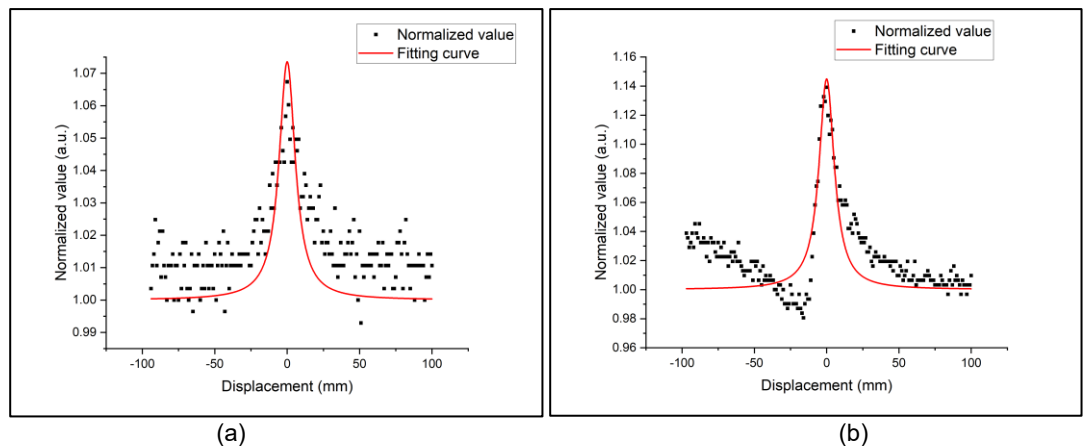


Figure 6. Fitted data from z-scan measurement for (a) TiO₂ and (b) BTiO_{2-x}

Q-Switched Performance

Figure 7 shows the OSA traces of both continuous wave (CW) and Q-switched outputs obtained. The CW output was taken without the SA in the cavity. In the CW mode, the laser's output wavelength was 1566.62 nm with a linewidth of 0.053 nm. For the TiO₂ SA Q-switched output, the output wavelength of the laser pulse shifted to the short wavelength at 1563.24 nm, and its linewidth was 0.096 nm. In contrast, the BTiO_{2-x} SA's wavelength and linewidth were 1565.75 nm and 0.212 nm, respectively.

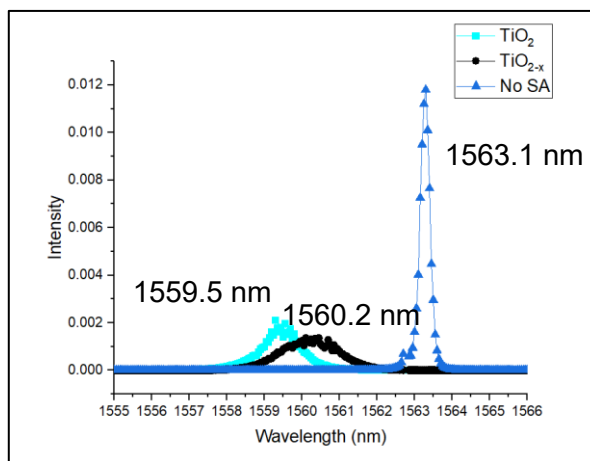


Figure 7. OSA traces of EDF laser outputs

Figure 8 shows the oscilloscope trace of the laser output pulses for the TiO₂ and BTiO_{2-x} SAs at a pump power of 76.05 mW. The repetition rates of the laser were 39.06 and 36.76 kHz for the TiO₂ and BTiO_{2-x} SAs, respectively.

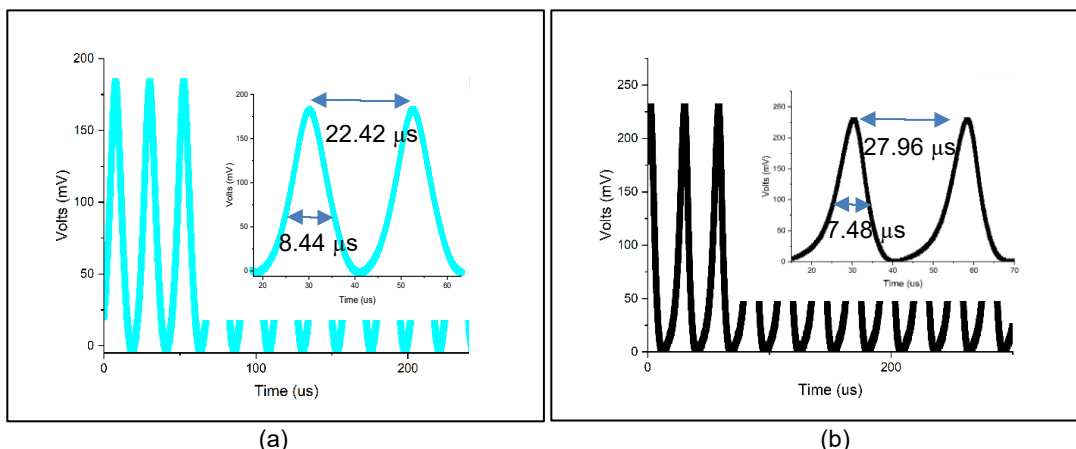


Figure 8. Oscilloscope traces at 76.05 mW pump power for (a) TiO₂ and (b) BTiO_{2-x} SAs.

The highest repetition rate achieved for the TiO₂ SA was 44.60 kHz with a pulse width of 8.44 μs, while for the BTiO_{2-x} SA, it was 35.77 kHz with a pulse width of 7.48 μs, as presented in Figure 9. Due to the higher nonlinear coefficient for BTiO_{2-x} SA compared to TiO₂ SA, shorter pulses can be achieved by compressing the pulses or controlling the pulse intensity modulation using nonlinear absorption. The performance of the laser outputs for the TiO₂ and BTiO_{2-x} SAs can be represented through the slope efficiency of the graph as shown in Figure 10 (a), which are 2.48 % and 2.22 %, respectively. The range of laser output power produced by the TiO₂ SA was 0.72 mW to 1.751 mW, while the BTiO_{2-x} SA generated output power from 1.401 mW to 2.367 mW. Furthermore, Figure 10 (b) represents the pulse energy produced by the TiO₂ was 26.79 nJ to 44.83 nJ when the pump power was increased from 85.21 mW to 126.48 mW. Similarly, the BTiO_{2-x} SA generated pulse energy of 52.69 nJ to 64.39 nJ when the power increased from 85.21 mW to 126.48 mW. From these results, BTiO_{2-x} is a better SA material than TiO₂ due to its ability to produce a shorter pulse width and higher pulse energy in the Q-switched operation.

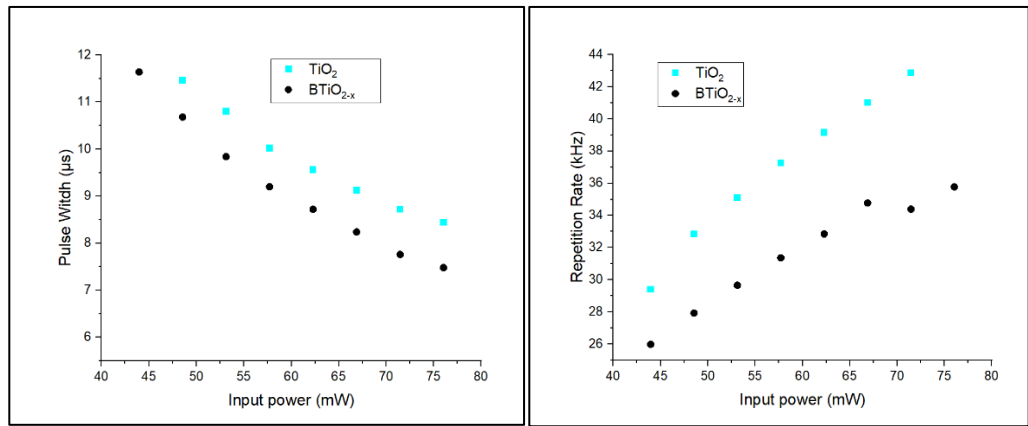


Figure 9. (a) Pulse width and (b) repetition rate as a function of pump power for TiO₂ and BTiO_{2-x} SAs

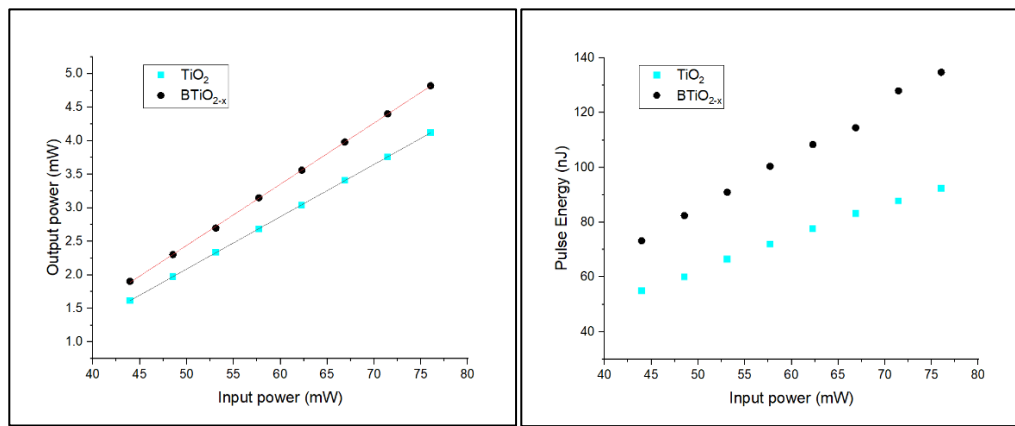


Figure 10. (a) Output power against pump power & (b) pulse energy against pump power graphs for TiO₂ and BTiO_{2-x} SAs

Figure 11 shows that when the pump power of the diode laser was increased, the peak power of the lasers for the TiO₂ and BTiO_{2-x} SAs also increased. TiO₂ and BTiO_{2-x} SA's peak powers increase from 4.33 mW to 13.71 mW and 6.29 mW to 22.32 mW, respectively. The higher peak power achieved by the BTiO_{2-x} SA is due to the combined effect of short pulse width and high pulse energy.

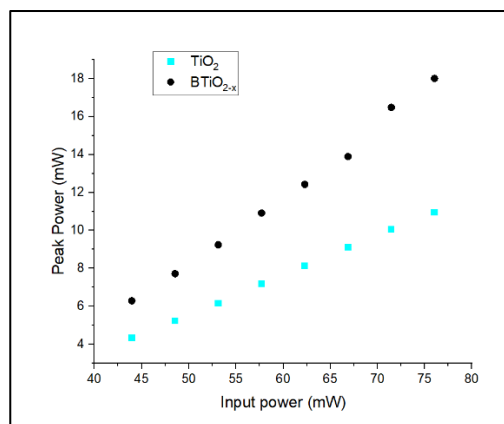


Figure 11. Peak power against pump power

Mode-locked Performance

Figure 12 shows the output power of mode-locked laser pulses produced by TiO_2 and BTiO_{2-x} SAs. TiO_2 SA has better slope efficiency in a mode-locked setup, about 37.72 %, compared to BTiO_{2-x} SA in Figure 12. However, due to the high threshold, TiO_2 SA needs higher pumped power to generate a mode-locked laser, contrary to BTiO_{2-x} SA, which requires only 62.29 mW of threshold pump power.

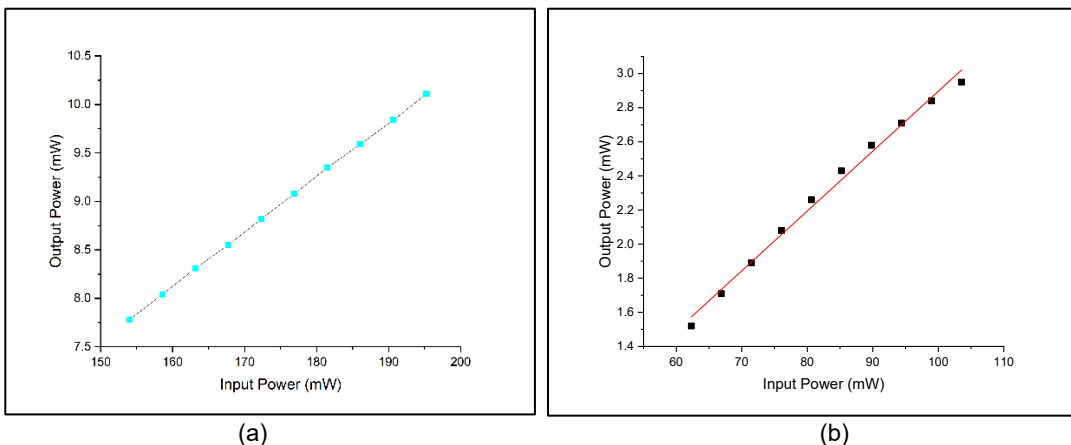


Figure 12. Output power against input power in mode-locked setup (a) TiO_2 and (b) BTiO_{2-x} SAs

Figure 13 shows that both SAs produced a consistent repetition rate of 1.87 MHz, demonstrating the laser's stability. Figure 14 (a) and (b) represent RF signals from both SAs, showing a stable mode-locked laser generation for TiO_2 and BTiO_{2-x} SA with signal-to-noise ratios of 52.04 dB and 41.47 dB, respectively. In addition, the RF signal recorded also shows that BTiO_{2-x} SA produced a more stable laser where the signal harmonics up to 40 MHz compared to TiO_2 up to 17 MHz.

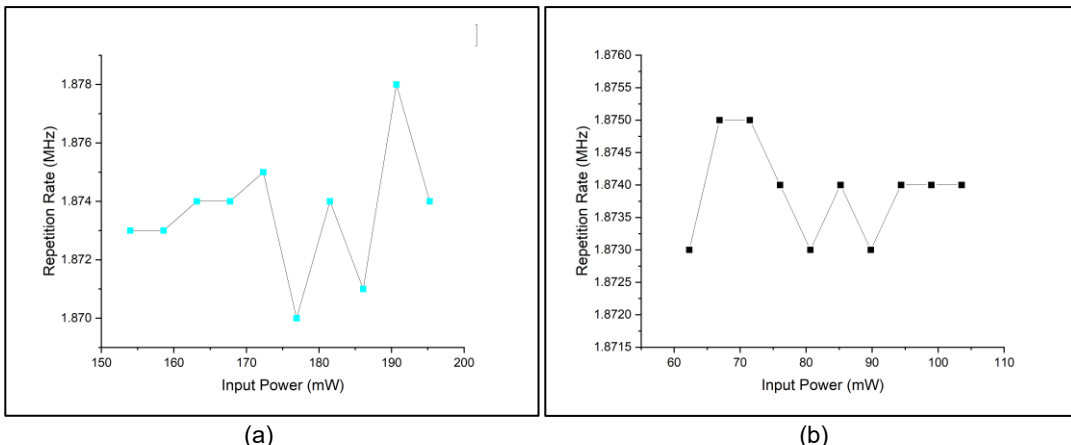


Figure 13. Repetition rate against pump power graphs for (a) TiO_2 and (b) BTiO_{2-x} SAs

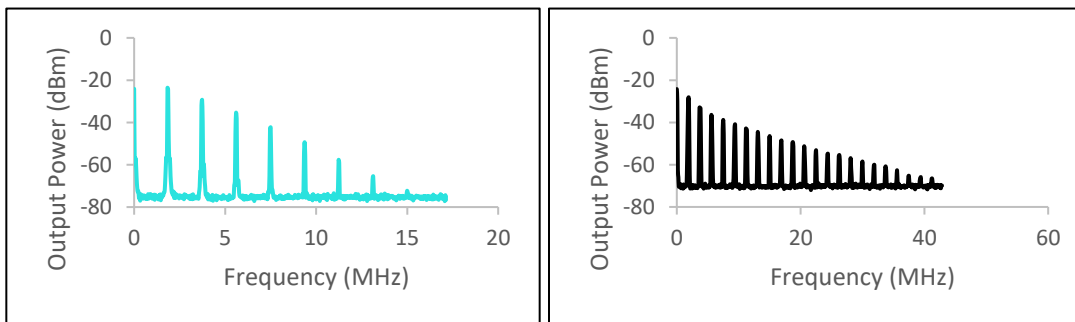


Figure 14. RF signals generated by (a) TiO_2 and (b) BTiO_{2-x} SAs

Figure 15 shows the autocorrelator data used to determine the mode-locked pulse width of the laser outputs produced. The mode-locked pulse widths produced from TiO₂ and BTiO_{2-x} SAs were determined to be 9.20 ps and 5.04 ps, respectively, as presented in Figure 15 (a) and (b). BTiO_{2-x} SA produces a shorter pulse width than TiO₂ SA, even though BTiO_{2-x} SA needs a lower pump power to generate a mode-locked laser. It shows the superiority of BTiO_{2-x} SA over TiO₂ SA in generating short pulsed laser output as a passive saturable absorber in mode-locked operation.

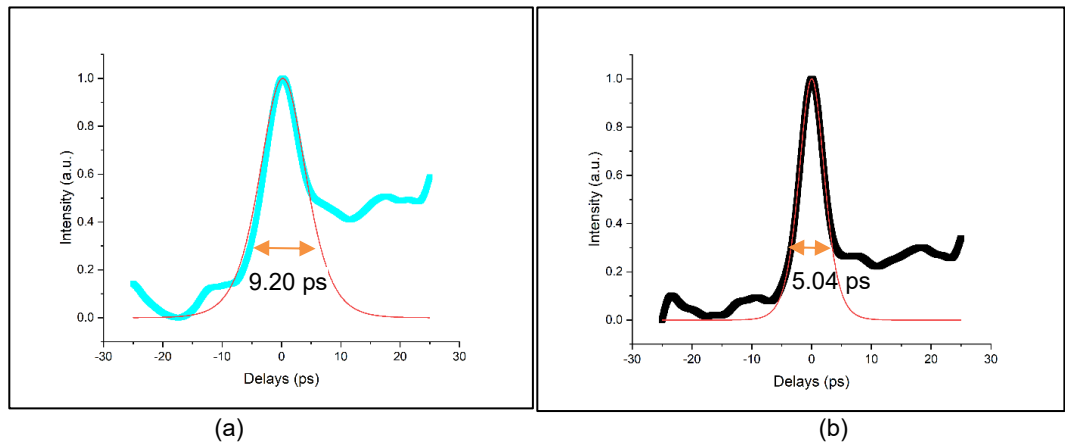


Figure 15. Pulse width generated in mode-locked by (a) TiO₂ and (b) BTiO_{2-x} SAs

Table 1 compares BTiO_{2-x} SA performance in this work with other SA materials in mode-locked operation. As indicated in Table 1, the BTiO_{2-x} SA performed better than the graphene SA in producing the shortest pulse width in the EDF laser system. Moreover, the BTiO_{2-x} SA was almost comparable with the zinc oxide SA in generating a high repetition rate pulsed laser. However, Ti₃SiC₂ MAX phase and Ti₃SiC₂ MAX phase SAs can produce much shorter pulse width compared to BTiO_{2-x} SA due to higher saturation intensity.

Table 1. Comparison of BTiO_{2-x} based saturable absorber lasing performance in mode-locked setup

SA Material	Pulse width (ps)	Repetition Rate (MHz)	Reference
Black Titanium Dioxide	5.04	1.8	This paper
Titanium Dioxide	9.2	1.8	This paper
Graphene	24 x 10 ³	5.78	[26]
SESAM	2 x 10 ³	0.2507	[27]
Tungsten disulphide	29.7	8.05	[28]
Zinc oxide	4 x 10 ⁵	1	[29]
Ti ₃ SiC ₂ MAX phase	3.03	1.88	[30]
MXene Ti ₃ C ₂ T _x	3.68	1.89	[31]

Conclusion

The BTiO_{2-x} thin-film SA had the potential to replace the TiO₂ as a saturable absorber in the EDF laser system, where it managed to modulate the laser to produce a better Q-switched pulsed laser. The results reveal that the slope efficiency using the BTiO_{2-x} SA had a lower efficiency of about 11.72 %. However, this SA produced higher output energy than the TiO₂ SA, which was about 60.9 % higher. Moreover, the highest pulse energy produced with BTiO_{2-x} SA was 64.39 nJ, which was 67.4 % better than TiO₂ SA. Introducing metal nanoparticles (NPs) in the BTiO_{2-x} SA could enhance the laser performance in pulse energy and peak power. The surface plasmon resonance of metal NPs should improve the absorption of photons, improving the Q-switching performance in the SA.

Acknowledgements

The authors would also like to thank the Ministry of Higher Education of Malaysia and Universiti Teknologi Malaysia for supporting their work with research funding via an International Matching Grant between Universiti Teknologi Malaysia and Universitas Negeri Malang Indonesia with a cost center number of R.J130000.7354.4B685. We especially thank the Research Management Center (RMC) of Universiti Teknologi Malaysia for managing the study funding.

References

- [1] R. Mary, D. Choudhury, and A. K. Kar. (2014). Applications of fiber lasers for the development of compact photonic devices. *IEEE J. Sel. Top. Quantum Electron.*, 20(5), 72-84. Doi: 10.1109/JSTQE.2014.2301136.
- [2] S. A. Sadeq, S. W. Harun, and A. H. Al-Janabi. (2018). Ultrashort pulse generation with an erbium-doped fiber laser ring cavity based on a copper oxide saturable absorber. *Appl. Opt.*, 57(18), 5180. Doi: 10.1364/ao.57.005180.
- [3] H. Guo *et al.* (2016). Q-switched erbium-doped fiber laser based on silver nanoparticles as a saturable absorber. *IEEE Photonics Technol. Lett.*, 28(2), 135-138. Doi: 10.1109/LPT.2015.2487521.
- [4] A. Nady, M. H. M. Ahmed, A. A. Latiff, A. Numan, C. H. Raymond Ooi, and S. W. Harun. (2017). Nickel oxide nanoparticles as a saturable absorber for an all-fiber passively Q-switched erbium-doped fiber laser. *Laser Phys.*, 27(6). Doi: 10.1088/1555-6611/aa6bd7.
- [5] N. A. Aziz, A. A. Latiff, M. Q. Lokman, E. Hanafi, and S. W. Harun. (2017). Zinc oxide-based Q-switched erbium-doped fiber laser. *Chinese Phys. Lett.*, 34(4), 2-5. Doi: 10.1088/0256-307X/34/4/044202.
- [6] M. A. A. B. Sahib, N. F. Zulkipli, A. H. A. Rosol, M. Yasin, and S. W. Harun. (2021). Titanium carbide MXene for generating Q-switched pulses in erbium-doped fiber laser cavity. *Microw. Opt. Technol. Lett.*, 63(11), 2893-2897. Ddoi: 10.1002/mop.32952.
- [7] M. Wang, C. Chen, C. Huang, and H. Chen. (2014). Passively Q-switched Er-doped fiber laser using a semiconductor saturable absorber mirror. *Optik (Stuttg.)*, 125(90), 2154-2156. Doi: 10.1016/j.ijleo.2013.10.047.
- [8] P. H. Reddy *et al.* (2018). Titanium dioxide doped fiber as a new saturable absorber for generating mode-locked erbium doped fiber laser. *Optik (Stuttg.)*, 158, 1327-1333. Doi: 10.1016/j.ijleo.2018.01.032.
- [9] Q. Bao *et al.* (2009). Large energy mode locking of an erbium-doped fiber laser with atomic layer graphene. *Adv. Funct. Mater.*, 19(19), 3077-3083. Doi: 10.1002/adfm.200901007.
- [10] Z. Luo *et al.* (2010). Graphene-based passively Q-switched dual-wavelength erbium-doped fiber laser. *Opt. Lett.*, 35(21), 3709. Doi: 10.1364/ol.35.003709.
- [11] D. Li *et al.* (2015). Polarization and thickness dependent absorption properties of black phosphorus: New saturable absorber for ultrafast pulse generation. *Sci. Rep.*, 5(Augst), 1-9. Doi: 10.1038/srep15899.
- [12] Q. Hu *et al.* (2019). Wavelength-dependent nonlinear absorption and ultrafast dynamics process of WS₂. *Opt. Express.*, 9(4), 1-9. Doi: 10.1364/osac.2.002755.
- [13] X. Jin *et al.* (2017). Wideband tunable ultrafast fiber laser using blackphosphorus saturable absorber. *2017 Opto-Electronics Commun. Conf. OECC 2017 Photonics Glob. Conf. PGC 2017*, 2017-Novem, 1-3. Doi: 10.1109/OECC.2017.8114937.
- [14] A. A. Latiff, M. F. M. Rusdi, M. B. Hisyam, H. Ahmad, and S. W. Harun. (2017). A generation of 2 μ m Q-switched thulium-doped fibre laser based on anatase titanium(IV) oxide film saturable absorber. *J. Mod. Opt.*, 64(2), 187-190, , doi: 10.1080/09500340.2016.1220641.
- [15] H. Ahmad *et al.* (2016). Band Q-switched fiber laser using titanium dioxide (TiO₂) as saturable absorber. *IEEE Photonics J.*, 8(1). Doi: 10.1109/JPHOT.2015.2506169.
- [16] Z. I. Rizman, B. A. Ahmad, M. F. M. Rusdi, Z. Jusoh, S. W. Harun, and M. Yasin. (2020). Tunable Q-switched erbium-doped fiber laser with titanium nanoparticles deposited onto PVA film as saturable absorber. *Nonlinear Opt. Quantum Opt.*, 52(3-4), 167-175.
- [17] N. Mohd Yusoff *et al.* (2020). Low threshold Q-switched fiber laser incorporating titanium dioxide saturable absorber from waste material. *Optik (Stuttg.)*, 18(May). Doi: 10.1016/j.ijleo.2020.164998.
- [18] N. Ahmed, N. H. Kamarulzaman, N. F. Zulkipli, Z. Jusoh, H. A. Rahman, and S. W. Harun. (2020). Generation of Q-switched Erbium-doped fiber laser using titanium dioxide film based saturable absorber. *IOP Conf. Ser. Mater. Sci. Eng.*, 854(1). Doi: 10.1088/1757-899X/854/1/012018.
- [19] J. Li *et al.* (2020). A facile method for the preparation of black TiO₂ by Al reduction of TiO₂ and their visible light photocatalytic activity. *RSC Adv.*, 10(57), 34775–34780. Doi: 10.1039/d0ra06784a.
- [20] L. Andronic and A. Enesca. (2020). Black TiO₂ synthesis by chemical reduction methods for photocatalysis applications. *Front. Chem.*, 8(November), 1-8. Doi: 10.3389/fchem.2020.565489.
- [21] R. F. Zhang, D. Z. Guo, and G. M. Zhang. (2017). Strong saturable absorption of black titanium oxide nanoparticle films. *Appl. Surf. Sci.*, 426, 763-769. Doi: 10.1016/j.apsusc.2017.07.222.
- [22] S. Cravanzola, F. Cesano, F. Gaziano, and D. Scarano. (2017). Sulfur-doped TiO₂: Structure and surface properties. *Catalysts*, 7(7). Doi: 10.3390/catal7070214.
- [23] L. S. Chougala, M. S. Yatnatti, R. K. Linganagoudar, R. R. Kamble, and J. S. Kadadevarmath. (2017). A simple approach on synthesis of TiO₂ nanoparticles and its application in dye sensitized solar cells. *Nano- Electron. Phys.*, 9(4), 2-7. Doi: 10.21272/jnep.9(4).04005.
- [24] H. Tan *et al.* (2014). A facile and versatile method for preparation of colored TiO₂ with enhanced solar-driven photocatalytic activity. *Nanoscale*, 6(17), 10216-10223. Doi: 10.1039/c4nr02677b.
- [25] M. Abdullah, H. Bakhtiar, S. Islam, M. S. A. Aziz, and G. Krishnan. (2019). Third-order nonlinearity and optical limiting properties of sol–gel-based bromophenol blue dye immobilized in silica–titania nanohybrid. *J. Sol-Gel*

- Sci. Technol.*, 89(2), 361-369. Doi: 10.1007/s10971-018-4906-5.
- [26] H. Xia *et al.* (2014). Nanosecond pulse generation in a graphene mode-locked erbium-doped fiber laser. *Opt. Commun.*, 330, 147-150. Doi: 10.1016/j.optcom.2014.05.048.
- [27] Shanghai jiao tong da xue. and Shanghai guang xue jing mi ji xie yan jiu suo. (2009). *CLEO/Pacific Rim 2009: the 8th Pacific Rim Conference on Lasers and Electro-Optics: Aug. 30-Sept. 3, 2009, Shanghai, China*. IEEE., Accessed: Jan. 09, 2023. [Online]. Available: https://opg.optica.org/abstract.cfm?uri=CLEOPR-2009-TUP3_11.
- [28] D. Mao *et al.* (2015). WS₂ saturable absorber for dissipative soliton mode locking at 106 and 155 μm . *Opt. Express*, 23(21), 27509. Doi: 10.1364/oe.23.027509.
- [29] I. A. M. Alani *et al.* (2019). Nanosecond mode-locked erbium doped fiber laser based on zinc oxide thin film saturable absorber. *Indian J. Phys.*, 93(1), 93-99. Doi: 10.1007/s12648-018-1251-z.
- [30] A. A. A. Jafry *et al.* (2020). MAX phase based saturable absorber for mode-locked erbium-doped fiber laser. *Opt. Laser Technol.*, 127(November), 1-8. Doi: 10.1016/j.optlastec.2020.106186.
- [31] S. W. H. A. H. A. Rosol, A. A. Aminuddin Jafry, B. Nizamani, N. F. Zulkipli, M. I. M. A. Khudus, M. Yasin. (2021). MXene Ti₃C₂T_x thin film as a saturable absorber for passively mode-locked and Q-switched fibre laser. *J. Mod. Opt.*, 68(18), 984-993. [Online]. Available: <https://doi.org/10.1080/09500340.2021.1967494>.